Identification and Characterization of an Intermediate Taxol Binding Site Within Microtubule Nanopores and a Mechanism for Tubulin Isotype Binding Selectivity

Holly Freedman,[†,‡] J. Torin Huzil,[†,‡] Tyler Luchko,[†,‡] Richard F. Ludueña,[§] and Jack A. Tuszynski*[,†,‡]

Department of Oncology, University of Alberta, Cross Cancer Institute, Edmonton, Alberta, Canada, Department of Physics, University of Alberta, Edmonton, Alberta, Canada, and Department of Biochemistry, University of Texas Health Science Center, San Antonio, Texas

Received September 12, 2008

Tubulin, the primary subunit of microtubules, is remarkable for the variety of small molecules to which it binds. Many of these are very useful or promising agents in cancer chemotherapy. One of the most useful of these is paclitaxel. The tubulin molecule is itself an α/β heterodimer, both α- and β-tubulin monomers existing as multiple isotypes. Despite the success of paclitaxel as an anticancer drug, resistance often occurs in cancer cells and has been associated with variations in tubulin isotype expression, most notably with the increased expression of βIII-tubulin. Paclitaxel is thought to reach its binding site on β-tubulin by diffusion through nanopores in the microtubule wall. It has been suggested that a transitional step in this process may be the binding of paclitaxel to an intermediate site within a nanopore, from which it moves directly to its binding site in the microtubule interior facing the lumen. To test this hypothesis, we have computationally docked paclitaxel within a microtubule nanopore and simulated its passage to the intermediate binding site. Targeted molecular dynamics was then used to test the hypothesis that paclitaxel utilizes the H6/H7 loop as a hinge to move directly from this intermediate binding site to its final position in the luminal binding site. We observed that this motion appears to be stabilized by the formation of a hydrogen bond involving serine 275 in β-tubulin isotypes I, IIa, IIb, IVa, IVb, V, VII, and VIII. Interestingly, this residue is replaced by alanine in the βIII and VI isotypes. This observation raises the possibility that the observed isotype difference in paclitaxel binding may be a kinetic effect arising from the isotype difference at this residue. We are now able to suggest derivatives of paclitaxel that may reverse the isotype-specificity or lead to an alternate stabilizing hydrogen-bond interaction with tubulin, thus increasing the rate of passage to the luminal binding site and hopefully offering a therapeutic advantage in paclitaxel resistant cases.

INTRODUCTION

Paclitaxel (Taxol) is a drug that is highly effective against solid tumors as a result of its antimitotic activity. The binding site for paclitaxel is located on the β-tubulin subunit within the α/β heterodimer, the repeating element forming the long protofilaments that together make up microtubule structures. It is the dynamic instability of microtubules that normally allows for their stochastic transitions from elongation to shortening (catastrophe) and vice versa (rescue), a process that is essential for the formation of the mitotic spindle followed by chromosome segregation during cell division. Shortening normally occurs when the GTP nucleotides, linking individual dimers, become hydrolyzed to GDP, causing dimers to depolymerize from the ends of the microtubule.[1] However, when paclitaxel binds to microtubules at its site within the lumen, the dynamic properties of the microtubules become altered, leading to the stabilization of tubulin against depolymerization.[2]

The paclitaxel-induced stabilization of microtubules is thought to occur through the strengthening of lateral contacts between adjacent protofilaments.[3] This stabilization may be a result of paclitaxel's interaction with the flexible M-loop on β-tubulin, resulting in its repositioning relative to the interprotofilament contact.[4] In the presence of paclitaxel, the M-loop is fixed in a conformation favorable to interaction between adjacent protofilaments.[5]

Several experiments have been designed in order to determine the mechanism by which paclitaxel gains access to its binding site on β-tubulin. While there has been some debate as to the possibility of paclitaxel entering through the open ends of the hollow cylinder constituting a microtubule,[6] the most recent evidence indicates that paclitaxel must enter the lumen by passing through the microtubule wall itself. Notably, Ross and Fygenson (2003) have carried out fluorescence recovery after photobleaching on microtubules to observe the diffusion patterns of fluorescently labeled paclitaxel derivatives.[7] They demonstrated a slower fluorescence recovery within thicker microtubule bundles and that the width of the bleached region changed little with time, indicating lateral diffusion of paclitaxel molecules. Additional evidence for the lateral diffusion of paclitaxel came from work by Buey et al.[8] who showed that the binding of cyclostreptin, a ligand known to bind at a site near the pore entrance, effectively inhibited paclitaxel binding to the microtubule lumen.

* Corresponding author e-mail: jtus@phys.ualberta.ca.
† Department of Oncology, University of Alberta.
‡ Department of Physics, University of Alberta.
§ University of Texas Health Science Center.

10.1021/ci8003336 CCC: $40.75
Published on Web 01/14/2009

Experimentally determined binding constants have been obtained by Diaz et al.,[9] who observed the diffusion of fluorescently labeled paclitaxel molecules to the binding sites. Their measured rate of binding was much larger than that which was estimated based on steric considerations and seemed to occur in two steps. The binding rate measured for the first step was $3.6 \times 10^6\ M^{-1}\ s^{-1}$, and the second step was observed to be slower. This measured kinetic rate constant seemed surprisingly high, given the relative inaccessibility of the binding site location to the solution surrounding the microtubules. In fact, Diaz et al.[9] estimated that passage through a cylinder about the size of microtubule pores would imply a binding rate at least 2 orders of magnitude smaller than that which was observed. The authors provided two possible explanations for the fast binding of paclitaxel. The first is that paclitaxel binds via large dynamic openings, continuously appearing as interprotofilament contacts rapidly change. However, this hypothesis was shown to be incorrect when fluorescence imaging showed no dark or bright spots,[10] and moreover cross-linked, frozen microtubules having more open holes in their walls displayed similar kinetics. The second hypothesis was that the paclitaxel binding rate being measured was to an intermediate site that is directly accessible to the bulk solution. Based on molecular modeling and a survey of mutations described in the literature as being associated with acquired resistance to paclitaxel, Diaz et al.[9] identified a potential intermediate binding site close to specific residues on the H6−H7 loop that differ in these mutant cell lines.

Because of the complex path involved in the binding of paclitaxel, a distinct possibility arises that paclitaxel binding to the luminal site can be influenced by individual residues near or within the nanopores, and, therefore, paclitaxel resistance could depend on the precise nature of these residues. It is worth noting that paclitaxel exhibits different degrees of efficacy in microtubules made from different human tubulin isotypes, highly homologous forms of tubulin encoded by different genes, that display differential expression patterns throughout the human body.[11] Interestingly, sequence variations between tubulin isotypes are not observed directly within the paclitaxel-binding site. This observation raises the possibility that differences in paclitaxel binding arise as a result of kinetics during its passage to its binding site and not due to differences in the binding energies at the final binding site, which is virtually identical. In the present work, we have used molecular modeling to characterize the putative intermediate binding site within the microtubule nanopores and investigated the path taken by paclitaxel from this site to the binding site within the microtubule lumen.

MATERIALS AND METHODS

Tubulin Model. The tubulin model used for all molecular dynamics calculations was based on 1TVK, a crystal structure solved at a 2.9 Å resolution for epothilone-bound tubulin in zinc-stabilized sheets.[12] 1TVK was chosen for its high resolution and being the most recent experimental structure that is compatible with a microtubule configuration. Also, since 1TVK does not include paclitaxel as a stabilizing ligand, when considering the feasibility of the proposed direct path from intermediate to final binding site, using this structure helps to avoid bias toward the final paclitaxel-bound configuration. Separate equilibration of the model in each of the intermediate and final binding sites as part of the molecular dynamics protocol further reduces any conformational bias.

A number of residues were not resolved in the 1TVK structure, namely the first residue and the carboxy-terminal tail of both monomers and residues 35 to 60 of α-tubulin. The C-terminal tails (residues 440 to 448 of α-tubulin and 428 and on of β-tubulin) were excluded from our final model. The remaining residues were placed in the 1TVK structure using Modeler 8v1[13] with residues 35 to 37 and 47 to 60 of α-tubulin taken from 1SA0.[14] A total of 1000 conformers for residues 38 to 46 were generated with the rest of the structure fixed. The lowest energy conformer was used as the initial structure for all molecular dynamics simulations. The position of the Mg^{2+} ion at the nonexchangeable site was taken from 1JFF[15] as it is not present in 1TVK.

Brownian dynamic calculations were done on microtubules created from models of isotypes αIV and βI, as described elsewhere.[16,17]

Microtubule Reconstruction. Tubulin dimers were placed in a configuration consistent with microtubule geometry by using the model of Li et al.[5] Specifically, by employing an in-house VMD[18] script, our tubulin dimer model was rotated about the protofilament axis 64° from the 1TVK orientation, aligning the microtubule radial axis with the z-axis of our coordinate system and the protofilament axis with the x-axis. Dimers were added laterally by rotating the new, duplicate dimer by 27.69° from its neighboring dimer about the microtubule center of mass, located 114 Å from the dimer center of mass, with a 9.2 Å longitudinal offset. Dimers were added longitudinally by offsetting the duplicate dimer 81.2 Å along the protofilament axis.

Paclitaxel Parameterization and Docking. Atomic charges for paclitaxel were determined by performing a Gaussian03[19] electronic structure calculation at the Hartree−Fock level. Due to convergence difficulties when attempting to use larger basis sets, the STO-3G basis set was used. Electrostatic potential fitting of atomic partial charges was performed by the Merz−Singh−Kollman method within Gaussian03. The parametrized paclitaxel ligand was then docked to the surface of the microtubule in each of the two pores by the AUTODOCK program,[20] using a cubic grid box with a spacing of 0.375 Å and dimensions of 70 Å. Using the Lamarckian genetic algorithm, 3×10^6 energy evaluations were performed for each of 100 trials. Clustering at 2 Å was used to obtain the final docked conformation of paclitaxel within the pore.

Brownian Dynamics. Brownian dynamics can be used to solve the Langevin equation ($ma = F - \gamma v + R$) for finite displacements made over discretized time intervals, where γ is the solvent-collision, or friction, parameter, and R is a random force vector such that $\langle R(t) \rangle = 0$. Here, in addition to forces arising from friction and stochastic motion, forces also arise from the electrostatic potentials surrounding the protein and the diffusing molecule, which were solved for from the Poisson−Boltzmann equation using the APBS software[21] at an ionic concentration of 150 mM. These potentials were stored as grids prior to simulations. Two million trajectories were run by following the sequence of

steps given below, which is implemented in the Simulation of Diffusional Association (SDA) computer program package:[22,23]

(i) The diffusing substrate is placed at random on the starting surface at a distance b from the binding site. The distance b must be chosen so that the force between the two molecules at this distance is independent of position on the surface.

(ii) The Ermak-McCammon equation is used to calculate the new center of mass and orientation using random displacement due to solvent collisions and the diffusion tensor. The new step is accepted only if there is no steric overlap between the diffusing molecule and the protein.

(iii) If the substrate has left an outer c-surface ($c > b$), the trajectory is truncated and counted as unsuccessful.

(iv) If the reaction criterion is met, the trajectory is truncated and counted as successful; otherwise a new loop is begun starting at step (ii).

The important information extracted from these simulations is the value of β, defined to be the number of successful trajectories divided by the total number of trajectories. Using β the rate of binding can be calculated from

$$k_{on} = k_{b,Sm}\rho = k_{b,Sm}\frac{\beta}{1-(1-\beta)\left({}^{k_{b,Sm}}/_{k_{c,Sm}}\right)} \quad (1)$$

where $k_{b,Sm}$ is the (Smoluchowski) rate at which particles at separation $r > b$ first strike b, and ρ is the probability that starting at b the drug reaches the binding site.

The SDA program was originally intended for modeling the association of diffusing proteins, with one of these starting on the surface of a sphere centered at the other. The SDA code had to be modified in our application to accommodate the cylindrical symmetry associated with diffusion of paclitaxel to the binding site on a microtubule. The on-rate is equal to the probability that starting on the surface of a cylinder the drug will end at the binding site times the rate at which particles hit the cylinder surrounding the microtubule coming from the outside. We used the result from Fick's law for the steady-state diffusion rate to the surface of an ellipsoid as an approximation to that for a cylinder, i.e. $k_{b,Sm} = (2\pi DL)/(\ln(L/b))$ where L is the length of the cylinder and b is its radius, in eq 1 when calculating the on-rate from the fraction of paclitaxel ligands reaching the binding site, as in the estimates made in ref 24. Periodic boundary conditions along the length of the cylinder were used to extend a single site on a cylinder to the diffusion to any of the microtubule's paclitaxel binding sites. The four tubulin monomers constituting a single pore were selected to be used as the protein structure containing the target binding site, following microtubule reconstruction as described above. We used values of 150 Å, 220 Å, and 4 μm, respectively, for b, c, and L. The microtubule radius from the axis to the center of geometry of the dimer is 114 Å, and with a pore depth of roughly 40 Å, this locates our outer cylinders at about 15 Å and 85 Å from the outer surface of the microtubule. The time step used was 1 ps, except at distances from the axis larger than 180 Å where it was increased linearly with separation.

Paclitaxel was modeled as a three-sphere dipole with radii determined as the effective electrostatic radii using the AMBER9 elsize program[25] and charges assigned by setting the dipole moment equal to that of paclitaxel, as shown in Figure S1 (Supporting Information). The dipole was composed of three points placed at the centers of mass of three groups of atoms, one of which corresponded to the C3 benzoyl group, another one to the side chain containing C2′ with its hydroxyl group and C3′ with its phenyl and benzoylamino groups, and the third one consisting of the remainder of the molecule including the tetracyclic core. Radii and charges are shown in the figure, and the distance between the central sphere and the two others were 8.1 Å and 6.2 Å, respectively. The exclusion radius for all dipole atoms, which must be uniform in SDA, was taken to be the largest of the three effective electrostatic radii, while for the protein exclusion, van der Waals radii were used and the exclusion grid was created with a spacing of 0.5 Å. Pairs of reacting atoms were chosen to consist of all combinations for which the distance between a protein atom and one of the three sites on the paclitaxel dipole is no more than 6 Å. To determine the translational and rotational diffusion constants of paclitaxel, the molecule was modeled as an ellipsoid and the formula of Bereolos et al.[26,27] was applied to give the values of 0.032 Å^2/ps and 4.7 $\times$ 10^{-3} rad^2/ps (the experimental value for the translational diffusion constant is 0.031 Å^2/ps). The linear density of microtubule sites was taken as 6.15 Å/site following ref 24.

Molecular Dynamics. Molecular dynamics (MD) was performed using the sander module of the AMBER8 program package.[28] Initial setup was performed in the leap and antechamber modules using the AMBER03 force field to parametrize the tubulin protein.[29,30] The MD simulations included two adjacent protofilaments composed of two tubulin heterodimers, containing the requisite GTP, GDP, and magnesium ions. Parameterization of nucleotide cofactors was taken from previously determined values.[31] Paclitaxel was placed at either the intermediate site within the pore or in the crystallographically determined binding site from the tubulin structure 1JFF,[15] and all atoms were represented using the charges described above and other parameters determined from the antechamber module of AMBER8. The protofilaments were then aligned with the x-axis in a periodic box with the x-dimension of the box set equal to 81.2 Å or the length of one tubulin dimer. Periodic boundary conditions were used and taken advantage of to model the system as two periodic protofilaments. A box of pre-equilibrated explicit TIP3P water[32] was added surrounding the solute with dimensions 81.2 Å by 107.5 Å by 152.5 Å; 64 neutralizing ions were also added. The water was then relaxed using 2000 steps of steepest descent, followed by conjugate gradient minimization. Following this, the entire system was then relaxed using another 2000 steps of steepest descent (600 steps) followed by conjugate gradient minimization. Next the system was heated to a final temperature of 300 K over a period of 10 ps using a Berendsen thermostat,[33] with restraints on all alpha carbons, the associated cofactors and paclitaxel, using a force constant of 50 kcal/mol. The SHAKE algorithm[34] was used to constrain bonds involving hydrogen in all simulations. Restraints were then gradually relaxed to zero over 25 ps with a time step of 1 fs. The time step was then increased to 2 fs, and a 1 ns production trajectory was generated.

In targeted molecular dynamics (TMD), a time-dependent harmonic restraint term is added to the energy based on the

root-mean-square deviation (rmsd) between the current structure and the target:

$$U_{TMD} = 0.5k_{ext}N(RMSD - RMSD_{target})^2 \quad (2)$$

where N is the number of atoms used in the root-mean-square difference calculation, k_{ext} is the external force constant, and the root-mean-square deviation (rmsd) is taken between the target structure and the current one. The target rmsd between the structure of paclitaxel in its current and final position in the luminal binding site was varied linearly from its initial value of 24.1 Å, with paclitaxel bound at the intermediate site in the pore, to 0 Å over the simulation period. Two separate TMD simulations were carried out in AMBER8,[28] one with the α-tubulin residues restrained by a harmonic potential with a force constant of 5 kcal/mol, which implicitly determined the fitting; we refer to this as Trajectory A. In the second simulation (Trajectory B), the fitting was to the β-tubulin residue having the bound paclitaxel in the luminal site in the target conformation. Qualitatively similar trajectories were observed in each of the two runs. To keep the constraint on the path followed by the drug relatively loose, we chose a force constant k_{ext} of only 1 kcal/mol to move the paclitaxel from the docked site in the pore to the binding site. Simulations were carried out over a period of 1 ns using a 2 fs time step, beginning with the structure obtained from equilibration and retaining the same explicit solvent.

Energy Calculations. MM-GBSA binding energy measurements were made using the MM-PBSA module of AMBER8, over the last 500 ps of the 1 ns runs with sampling every 10 ps. Binding free energies were determined as the sum of solvation free energy differences and gas-phase energy differences between the separated drug/protein system and the complex. The computational glycine scanning functionality of MM-PBSA was used to evaluate the specific contribution of β-tubulin residue Ser 275 to binding; although alanine scanning is more commonly used experimentally, the program requires that serine be mutated to a smaller residue than itself, hence the use of glycine scanning. Additionally, MM-GBSA binding free energies were calculated as a function of progress in the targeted molecular dynamics simulation from Trajectory B, and loop energies were found by running the anal module of AMBER8 on coordinate files taken from the same trajectory. All other results of TMD including figures were taken from Trajectory A. The ptraj module of AMBER8 was used in the interatomic distance analyses.

RESULTS

Modeling of Microtubule Nanopores. Tubulin is a globular heterodimer. This means that any lateral arrangement between rows of tubulin molecules will create pores along the interface of their connection. One pore (nanopore 1) is located in the region where the interdimer α/β interface of one tubulin molecule lies next to the interdimer α/β interface of the adjacent tubulin molecule. A second, apparently smaller, nanopore (called nanopore 2) arises where the α/β intradimer interface of one tubulin molecule lies next to the α/β intradimer interface of the adjacent tubulin molecule. In addition to these two pores, which fit well in the type B lattice, microtubules also contain a "seam", part of a type A lattice; two analogous nanopores, designated 1s and 2s, would be located along this seam (see Figure 2).

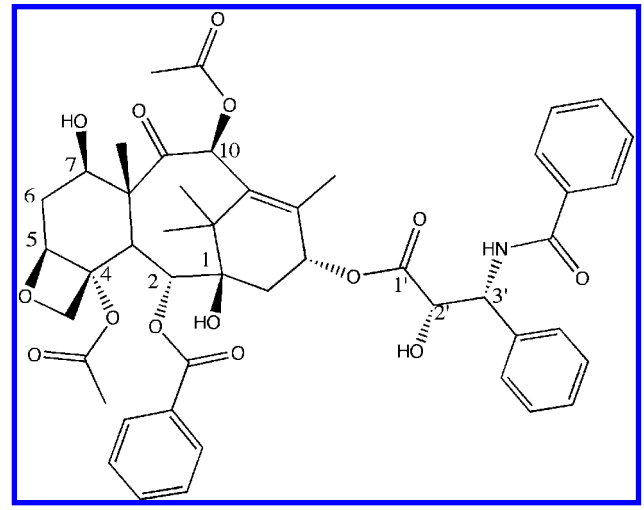

Figure 1. Structure of paclitaxel, showing atom numbering scheme.

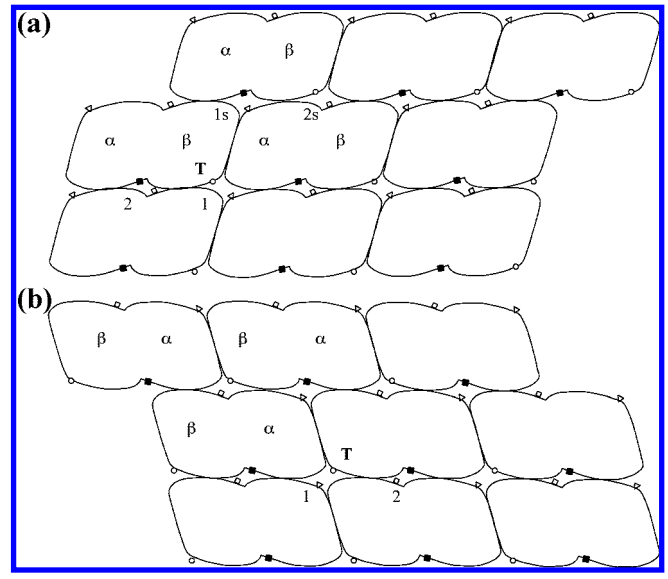

Figure 2. Schematic representations of the outside (a) and inside (b) view of the microtubule wall surface. White and black squares represent residues β ASP 128 and α ASP 218, respectively, while the triangle stands for α THR 130 and the circle for β PHE 212. The letter "T" marks the paclitaxel binding site.

Here, the bottom and middle protofilaments come together to form the B lattice configuration, typical of most microtubules. Only the interface between the top protofilament and the second one down (the microtubule seam) is commonly comprised of an A lattice. In the type B lattice, pores of type 1 were observed to be larger than type 2 pores and also appear larger than the two pore types seen at the seams. All residues that line each of the four pore types are listed in Table S1 (Supporting Information).

The type 1 nanopore is the closest to the paclitaxel-binding site and is presumably where paclitaxel most likely enters to access the binding site. We measured the point of closest constriction in this pore; considering heavy atoms only, this corresponds to the distance between the CZ atom of β PHE 212 and CG2 of α THR 130 and ranged from 10.1 to 10.7 Å. Although slightly different values were obtained when examining different isotype models, this was caused by different side chain rotamer states, rather than actual differences between isotypes. For pores of type 2, distances of 10.5 to 11.4 Å or 9.6 to 12.7 Å were obtained for

measurements taken between β ASP 128 and each of the two α residues ASP 218 and GLU 220, respectively. For pores along the seam of type 1s, distances measured between α THR 130 and ASP 218 of the opposite α tubulin ranged from 9.7 to 9.9 Å, and for those of type 2s, distances between β PHE 212 and ASP 128 of the opposite β-tubulin varied from 8.0 to 9.9 Å.

Since paclitaxel most likely traverses the type 1 pore, the residue differences in this pore among β-tubulin isotypes I, IIa, IIb, III, IVa, and IVb were examined. Several of the residue substitutions are seen in one cluster at the outer edge of the wide luminal opening of β subunit 2, including residues 33 and 55−57. However, no differences are observed on the outer rim, and only two are observed in the interior of the pore. Specifically, a substitution of T218A on the H6/H7 loop of β subunit 1 is observed in βIII microtubules, and S115A of β subunit 2 is observed in βIVa microtubules. Among the substitutions observed between isotypes, it seems unlikely that any except S115A, discussed below, would significantly affect the ability of paclitaxel to access its binding site. Calculation of the electrostatic potential grid surrounding the pores shows that the potential is substantially more negative on the outside of the pore than on the inside (see Figure 3).

Paclitaxel Flexibility. Paclitaxel is a relatively large molecule with four side chains extending from its main multiring structure (see Figure 1a). It is possible that its internal flexibility may contribute to reduced van der Waals overlap during its motion to the binding site. One way of quantifying this flexibility is by comparing the energies of conformers relative to the distances between functional groups. From such an analysis of the structure of the implicitly solvated drug, a change of 1 kcal/mol above the lowest energy state was found to correspond to increasing or decreasing the distance between the C2-benzoyl group, and a second group containing both C3′-phenyl and benzoylamino side chains, by as much as 3 Å from the minimum of 12 Å; with the same energetic penalty, the narrower dimension between the two close C3′-phenyl and benzoylamino rings may be varied from its minimum energy value of 6.6 Å by about 0.5 Å.

Location of the Intermediate Binding Site. Figure 4 shows a histogram of results obtained from performing automated docking of paclitaxel in each of the two types of pores, clustered at an rmsd of 2 Å. These results give no indication of paclitaxel binding within the type 2 pore. On the other hand, for the type 1 pore the lowest energy cluster is also the largest, with 24 elements and a lowest docked energy of −16.31 kcal/mol; moreover, upon examination all results in this cluster show paclitaxel in the same orientation, that is this cluster represents a single conformation. The existence of this large cluster gives support to the proposed existence of an intermediate binding site in the pore. Moreover, the paclitaxel position and conformation within this cluster is located under the H6/H7 loop in a position similar to that previously predicted by Diaz et al.[9] Interestingly, this binding site is physically separated from the luminal binding site by the M-loop, which is normally associated with microtubule stabilization upon addition of paclitaxel.[3,4] The location of the resulting intermediate binding site relative to the observed binding site, following equilibration by molecular dynamics simulation, is shown in Figure 5. Tubulin isotype substitutions near this site that are known to confer reduced sensitivity or resistance to paclitaxel include L215H, L215V, L215I, and L217R in the H6/H7 loop and T274I and R282N on the M-loop.[35−40] As shown in Figure 5, these residues are located between the two paclitaxel binding sites; while Leu 217 likely stabilizes paclitaxel when bound in the lumen, and Thr 274 is also close enough to the luminal binding site to potentially stabilize this binding, residues Leu 215 and Arg 282 are not part of the luminal binding site and so another explanation for the effects of mutating these residues is needed. These residues could potentially be critical for paclitaxel's binding at the intermediate site within the pore or in its transition to the observed binding site.

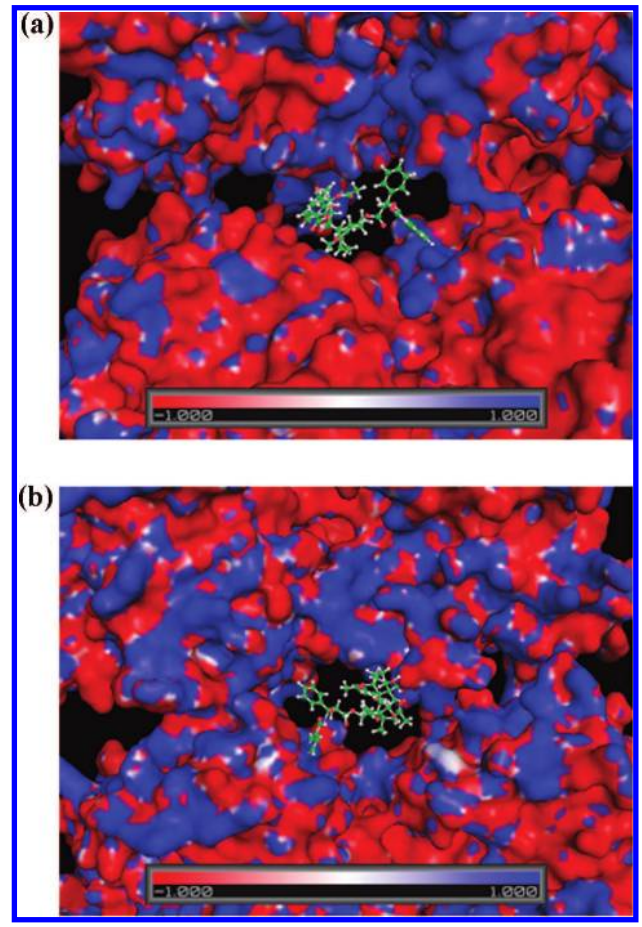

Figure 3. Solvent accessible surface of the type 1 pore in an αIV/βI microtubule colored by electrostatic potential viewed from the outside (a) and inside (b), visualized using the Pymol viewing program.[64] The scale gives the color range for the electrostatic potential in *kT*. Orientations are as in parts (a) and (b), respectively, of Figure 2 for pore 1. Paclitaxel has been overlaid in the openings to illustrate the drug's dimensions relative to those of the pore, showing that steric considerations are quite restrictive as far as letting paclitaxel traverse the pore.

Calculation of Mean Free Passage Time. Because the measured rate of paclitaxel binding to microtubules is inversely proportional to the solvent viscosity, it is thought to be a diffusion-controlled process.[9] Brownian dynamics may therefore appropriately be used to model this binding pathway. Brownian dynamics simulations have been used to determine rates of diffusion-controlled binding events, including protein−protein interactions.[22,23] The rate calculated for paclitaxel binding to microtubules by Brownian

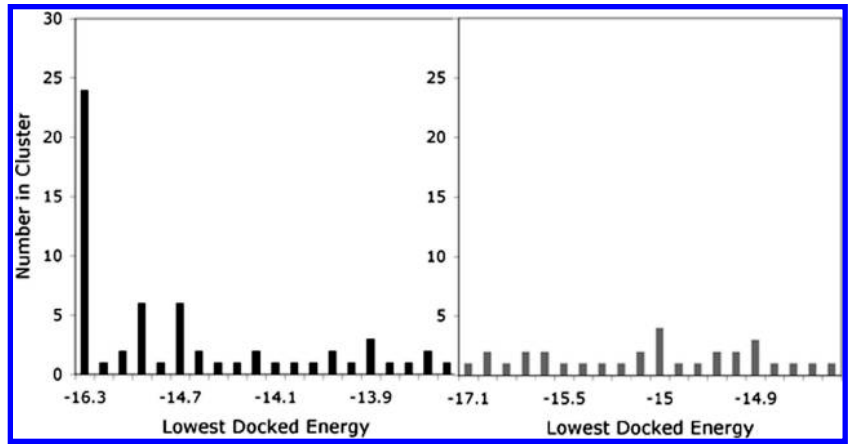

Figure 4. Histogram showing the energies and numbers of elements of clusters obtained from docking paclitaxel within the type 1 microtubule pore (left panel) and the type 2 pore (right panel).

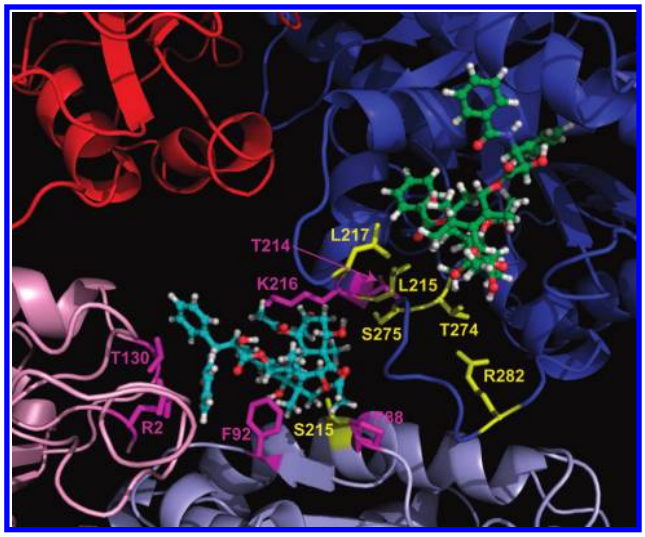

Figure 5. Model of type 1 nanopore, comparing positions of paclitaxel, colored in light green and teal, respectively, at each of two binding sites, the observed binding site and the proposed intermediate binding site. β-Tubulin units are colored in blue and blue-gray, and α-tubulin units are red or light pink. The residues involved in paclitaxel-resistant point mutations or isotype differences are colored in yellow, while contacts within 6 Å contributing most significantly to binding at the site in the pore are shown in pink; note that serine 215 belongs to both classes.

dynamics may be compared to that which has been measured experimentally.

Our initial attempts to use an all-atom model for paclitaxel in Brownian dynamics simulations demonstrated that steric restraints would require modification of probe radii in order to implicitly allow for some flexibility. However, when somewhat decreased values of the atomic exclusion radii were employed to avoid steric overlap with the protein, increased electrostatic interactions caused paclitaxel to stick to the protein surface and led to rates 2 or 3 orders of magnitude too small (not shown). As a result, we chose to employ a more simplified model of paclitaxel as a three-point dipole as described in the Methods section. The dipole consists of two positive point charges located at the C2 benzoyl and at the C2′/C3′-linked side chains, respectively, and one negatively charged point representing the main paclitaxel ring complex (see Figure S1, Supporting Information).

In Figure 6, the calculated rate of interaction is shown as a function of contact distance of from one to four sites. For protein association calculated by the SDA program, the reaction criterion is generally defined as two contacts at a distance of 6.0−6.5 Å (with an all-atom representation).[23] The smallest contact distance seen here was at 6.5 Å, and for this distance the rate found for two contacts was 3.70×10^6 M^{-1} s^{-1}, with a standard deviation of 5.76×10^5 M^{-1} s^{-1} based on four data subsets. This value is in excellent agreement with the value of 3.6×10^6 M^{-1} s^{-1} measured for paclitaxel binding to microtubules by Diaz et al.[9] Note that the rates for either one or two contacts are practically identical, although for more contacts the rates are significantly less. This demonstrates that although our model seems to give an accurate representation of the passage of the drug to roughly the point of the binding site in the pore, the drug generally is not assuming its correct orientation by forming more than two of the correct contacts at the binding site in the simulations, at least partially as a result of the tight constriction within the pore. This may be expected to introduce some error into the results, although we still see excellent agreement between our estimated rate and the experimental value of the kinetic rate constant for paclitaxel association.

To assess the role of electrostatics in contributing to the ability of paclitaxel to bind to microtubules, the same calculations were repeated, but this time with all interactions turned off except for the exclusion forces. The calculated rate at which two contacts were formed at 6.5 Å was 3.20×10^6 M^{-1} s^{-1} with a standard deviation of 7.38×10^5 M^{-1} s^{-1}, i.e. there was very little difference indicating negligible influence on binding from any but purely diffusive factors.

Binding Free Energy Calculations. Using the latter halves of one-nanosecond trajectories for each site, we calculated the binding free energies at the intermediate and luminal sites to be −26.38 kcal/mol and −43.28 kcal/mol, respectively, for the βI, αIV isotype pair with standard deviations of 4.68 and 3.11 kcal/mol. Because the unfavorable conformation entropy change upon binding was not included in our calculations, these values overestimate the magnitude of the binding energies, although they provide a rough idea of the relative strengths of the two binding interactions.

In addition, we decomposed the binding free energy at the intermediate site according to receptor residue for those residues within 6 Å of the ligand (see Table 1). Some of the largest contributions to the binding energy are made by

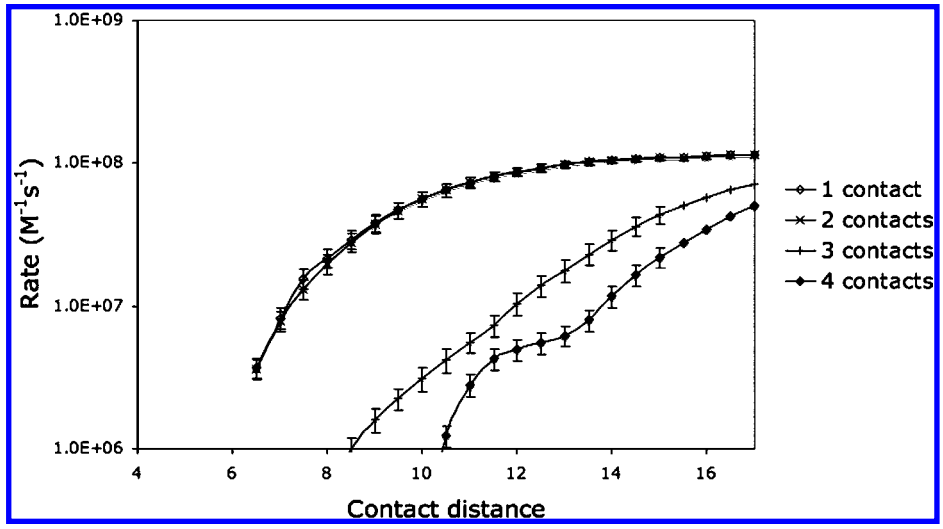

Figure 6. SDA-calculated rate-constants for paclitaxel binding to the proposed intermediate binding site within the microtubule pore, with error bars representing standard deviations over 4 data subsets.

Table 1. Contributions of Individual Residues within the Intermediate Binding Site (Defined by 6 Å Criterion) to Binding Free Energy at the Intermediate Binding Site[a]

	residue	$\Delta\Delta G_i$	$\Delta\Delta G_{i,solv}$	$\Delta\Delta G_{i,gas}$
beta 2	PRO 70	−0.83	−0.31	−0.52
	PRO 88	−2.98	−2.87	−0.11
	ASN 89	0.06	0.13	−0.07
	PHE 90	−0.92	−0.12	−0.8
	VAL 91	−1.43	−0.26	−1.17
	PHE 92	−8.15	−2.81	−5.34
	GLY 93	−0.74	−0.19	−0.55
	GLN 94	−2.28	0.01	−2.29
	GLU 111	−1.61	−0.73	−0.88
	LEU 112	−2.41	−1.19	−1.22
	VAL 113	0.13	0.16	−0.03
	ASP 114	−0.23	−1.00	0.77
	SER 115	−2.87	−0.68	−2.19
alpha	ARG 2	−3.16	−2.08	−1.08
	GLN 128	−0.10	−0.00	−0.1
	CYS 129	−0.65	−0.10	−0.55
	THR 130	−5.16	−2.33	−2.83
	GLY 131	−0.24	−0.09	−0.15
beta 1	PHE 212	−1.89	−0.64	−1.25
	ARG 213	−1.23	−0.10	−1.13
	THR 214	−2.81	−0.58	−2.23
	LEU 215	−1.95	−0.02	−1.93
	LYS 216	−5.56	−1.03	−4.53

[a] In kcal/mol. Of the two β-tubulin subunits, beta-1 refers to the one with taxol bound in the luminal site.

Table 2. Contributions of Individual Residues within the M-Loop to Binding Free Energy at the Intermediate and Final Binding Sites[a]

	intermediate binding site			final binding site		
residue	$\Delta\Delta G_i$	$\Delta\Delta G_{i,solv}$	$\Delta\Delta G_{i,gas}$	$\Delta\Delta G_i$	$\Delta\Delta G_{i,solv}$	$\Delta\Delta G_{i,gas}$
PHE 270	0.01	0.00	0.01	−1.26	−0.71	−0.56
ALA 271	0.02	0.00	0.02	0.09	0.00	0.08
PRO 272	0.00	0.00	0.00	−0.50	−0.57	0.07
LEU 273	0.05	0.03	0.02	−2.93	−0.49	−2.44
THR 274	0.12	0.21	−0.09	−4.68	−1.64	−3.05
SER 275	−0.51	−0.10	−0.41	−0.08	0.17	−0.26
ARG 276	−0.04	0.15	−0.19	−0.99	2.91	−3.90
GLY 277	0.01	0.04	−0.03	−1.58	−0.46	−1.12
SER 278	−0.04	0.18	−0.22	−0.21	−0.11	−0.10
GLN 279	0.14	0.48	−0.34	0.09	0.08	0.02
GLN 280	−0.01	0.02	−0.03	0.01	0.02	−0.01
TYR 281	−0.44	−0.28	−0.16	−0.02	0.01	−0.03
ARG 282	0.06	0.68	−0.62	0.05	0.65	−0.60
ALA 283	0.00	0.00	0.00	0.01	0.02	−0.02
LEU 284	0.00	0.03	−0.03	−0.10	0.04	−0.14
THR 285	0.00	−0.01	0.01	−0.03	−0.01	−0.02
VAL 286	0.01	0.00	0.01	0.01	0.02	−0.01

[a] In kcal/mol.

residues within the β-tubulin H6/H7 loop. Thr 214 and Lys 216 of the β-tubulin containing the paclitaxel luminal binding site, Pro 88, Phe 92, and Ser 115 of the opposite β-tubulin, and Arg 2 and Thr 130 of the opposite α tubulin, make the largest contributions to binding, mostly by increasing the nonsolvated interaction energy, although in the case of Pro 88 the desolvation upon binding is the main cause of stabilization (see Table 1 and Figure 5). It is interesting to speculate on the role played by the S115A substitution in βIVa, mentioned above, in the reduced sensitivity to paclitaxel that has been observed in microtubules composed of this isotype,[41] since this residue makes a significant contribution to the binding of paclitaxel in the pore by hydrogen-bonding with the carbonyl oxygen of paclitaxel's C2-benzoyl group. Table 2 shows that the residues of the M-loop contribute little to the thermodynamic stability of the intermediate paclitaxel/tubulin complex.

Contributions of individual residues in the M-loop to the paclitaxel binding free energy at the luminal site are also shown in Table 2. The contribution from Serine 275 is only −0.1 kcal/mol, and thus the role of this residue in stabilizing the binding may be expected to be negligible; it may be noted that several residues of the M-loop do in fact make major contributions to binding here. In addition, we used the computational glycine scanning to test for the importance of β-tubulin Ser 275 to the binding at each site. Binding energies calculated with glycine scanning were −26.2 kcal/mol and −43.1 kcal/mol at the sites in the pore and in the lumen, respectively, thus hardly differing from those with the serine at position 275 in either case. Thus it is unlikely that the binding contribution of this residue alone would affect paclitaxel activity when Ser 275 is substituted for by an alanine as in βIII microtubules.

Contributions to binding free energy at the final binding site from residues within 6 Å of the ligand are tabulated in the Supporting Information.

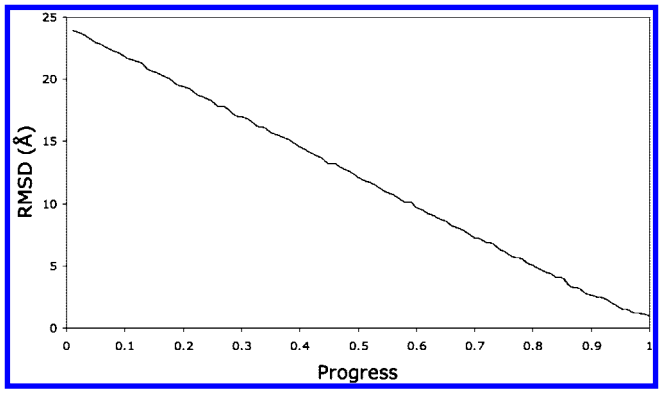

Figure 7. rmsd from target position as a function of simulation progress.

Targeted Molecular Dynamics between Binding Sites. Diaz et al.[9] suggested that the H6−H7 loop might serve as a hinge to facilitate the passage of paclitaxel directly from the intermediate binding site to the observed binding site. To model such a process, an accelerated dynamics approach is needed. In targeted molecular dynamics the magnitude of the force depends on the rmsd between the initial and target orientation.[42] Although the minimum-energy path will not necessarily be obtained by this method, it seemed a well-suited method for testing the feasibility of and qualitatively observing the proposed motion; other accelerated molecular dynamic methods also exist including steered molecular dynamics,[43] which however requires a prior identification of the reaction coordinate, and umbrella sampling, which is extremely computationally intensive.

In Figure 7, the rmsd relative to the final binding position is plotted as a function of simulation progress, the latter being defined as the fraction of total simulation time so far completed. Introducing a restraint of 1 kcal/mol was successful in forcing the trajectory of paclitaxel to adhere closely to the linear trend defined by the target rmsd; a slight exception may be seen at the end of the trajectory where the rmsd remains positive. Figure 8 depicts continuously spaced snapshots from start to finish of the TMD trajectory. Our analysis of the TMD trajectory shows that the M-loop of β-tubulin follows the motion of the drug, being pulled by the interactions between drug and protein during the hinging motion. This observation is particularly interesting considering the function paclitaxel has been hypothesized to have in fixing the position of the M-loop, hence promoting microtubule stability. Furthermore, it was observed that the pathway is marked by a hydrogen bond between paclitaxel's C7-hydroxyl and the side chain hydroxyl of serine 275 on the M-loop of the β-tubulin subunit containing the binding site. This hydrogen bond may be partially responsible for the stabilization of binding during the transfer of paclitaxel from the pore to the lumen. Figure 9a shows how the distance between hydroxyl HG of Ser 275 and hydroxyl O7 of paclitaxel varies over the course of the simulation. Residue 275 is not hydrogen bonded to paclitaxel in the intermediate site but only draws near to it during the hinging motion and transfer through the pore. As can be seen in Figure 9a, a hydrogen bond, which typically corresponds to a distance of about 2.8 Å, persists throughout the second quarter of the simulation. As paclitaxel approaches the luminal binding site in the simulation, the hydrogen bond with the side chain of Ser 275 is substituted for by one with the main chain carbonyl of this residue as the position of paclitaxel shifts relative to the M-loop.

Kinetics of Transfer. An obvious question that should be addressed is the kinetic feasibility for the occurrence of the proposed motion within a biologically relevant time frame. Although this is difficult to determine exactly from TMD, one can approximate it by examining the binding free energies along the trajectory (see Figure 10a). The magnitude of the observed barriers (not more than about 15 kcal/mol) indicates that the motion should be feasible on a time scale of possibly hundredths of seconds. However it is necessary to also consider the possibility that the energetics associated with the accompanying motion of the tubulin may lead to a large additional kinetic barrier. Figure 10b shows the potential energy of the H6/H7 loop with flanking residues included. A wide spread of energies is seen representing the lack of proper equilibration, but judging from the minimum energies there does not seem to be a significant barrier to the motion resulting from this energy until the end of the trajectory, when the position of the paclitaxel and the artificially imposed restrictions to motion imposed by the driving force trap the H6/H7 loop and prevent it from relaxing. Thus, as far as could be determined from our simulations, the motion of the loop does not present a large obstacle to the motion of paclitaxel between the two sites, and the transfer of paclitaxel is likely to be rapid.

DISCUSSION

Tubulin Isotypes. In many normal human cells βI is the prevalent isotype, while βIII and βII are seen in higher proportions in cancer cells.[44−50] For cancer cells with changes in isotype composition, only the increase in βIII microtubules has been shown to be associated with paclitaxel resistance.[51−55] Moreover, it has been demonstrated that paclitaxel has a stronger effect in reducing the dynamics of microtubules in βII or unfractionated microtubules compared to βIII or βIV microtubules.[41] This is also supported by evidence that paclitaxel is more effective at stabilizing microtubules depleted of βIII[56] and less effective at stabilizing microtubules composed solely of βIII tubulin.[57] How at the molecular level drug resistance to paclitaxel occurs due to overexpression of βIII tubulin is an unsolved question, which we now attempt to address.

When considering isotype differences, the one that is closest to the observed binding site of paclitaxel is in position 275; this residue is a serine in β isotypes IIa, IIb, IVa, IVb, V, VII, and VIII but is an alanine in βIII and VI. In the crystal structure, this residue does not seem to directly interact with the bound paclitaxel molecule. However, based on the results of computer simulations, Magnani et al.[58] have argued that the stronger effect paclitaxel has in reducing the dynamics of microtubules in unfractionated microtubules compared to βIII microtubules is the result of the contribution made by residue Ser 275 to the binding affinity at the luminal binding site. By contrast, our results indicate that Ser 275 makes little if any thermodynamic contribution to binding.

A second possibility, namely that βIII microtubules resist stabilization by paclitaxel as a result of generally increased dynamic instability, is also ruled out by a recent study demonstrating that microtubules composed of βII and βIII have almost identical rates of polymerization and depolym-

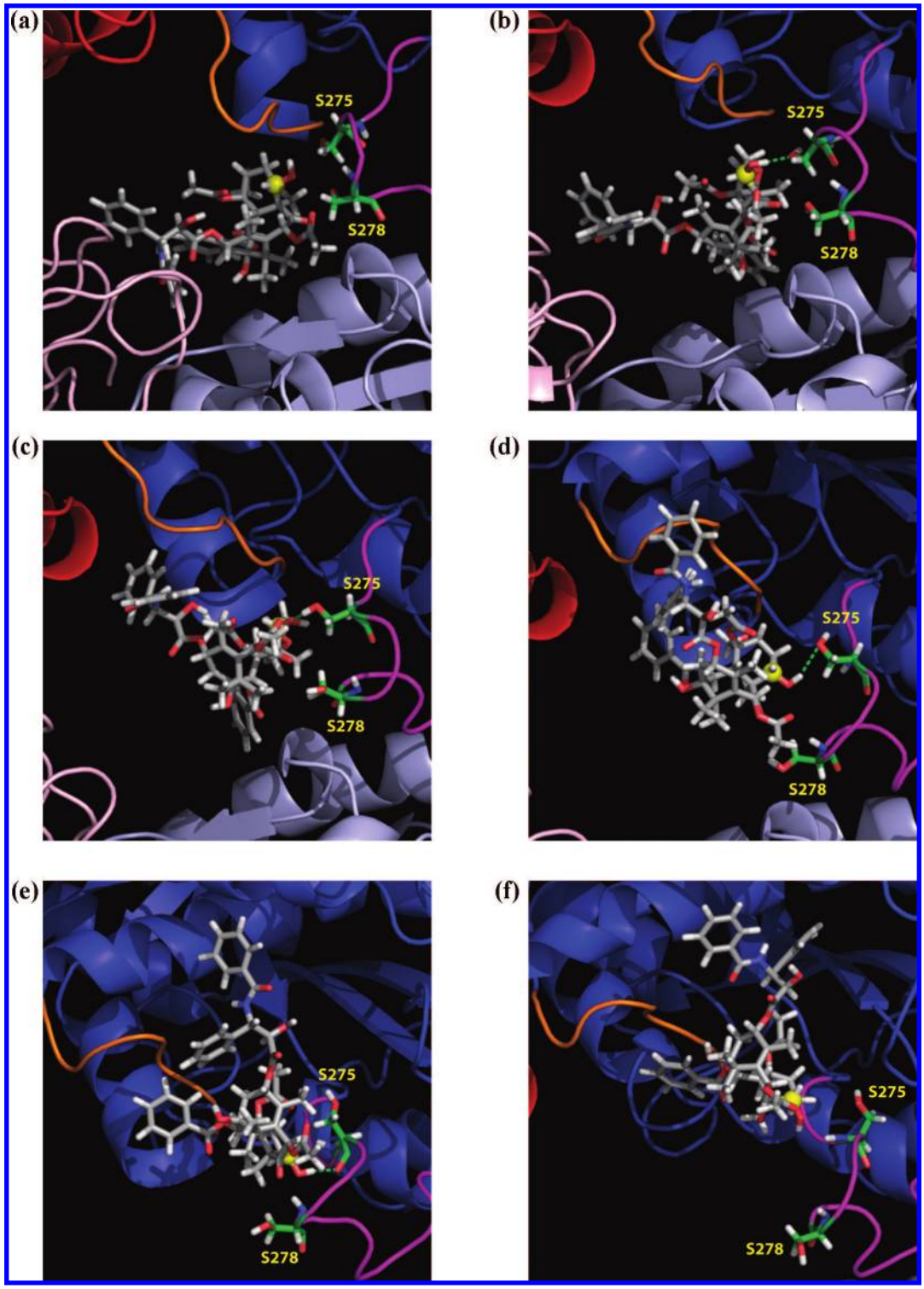

Figure 8. Snapshots extracted from the targeted molecular dynamics simulation at simulation progress values of (a) 0, (b) 0.2, (c) 0.4, (d) 0.6, (e) 0.8, and (f) 1.0. The M-loop is shown colored in pink, and the H6/H7 loop is in orange.

erization.[59] In that study the main isotype-difference seemed to relate to the amount of time spent in attenuation, and even this difference was subtle. The work of Kamath et al.[52] demonstrating that strong overexpression of βIII tubulin does not lead to increased microtubule dynamics also disproves the explanation that isotype composition may effect microtubule dynamics even in the absence of paclitaxel. Rather, existing evidence indicates that intracellular conditions such as concentrations of associated proteins are likely the major determining factors in the variability of microtubule dynamics.[60]

Kinetic differences in drug binding provide another possible explanation for the observed isotype specificity of paclitaxel. In the present study, we observed a stabilizing hydrogen bond between paclitaxel and Ser 275 of β-tubulin. We predict that the reason for the greater effectiveness of paclitaxel in βII compared to βIII microtubules is the lowering of the barrier height for the motion of paclitaxel between the two binding sites caused by the hydrogen bond between O7 and the serine at position 275.

When comparing dynamics suppressivity of different isotypes by paclitaxel, Derry et al.[41] state that their measure-

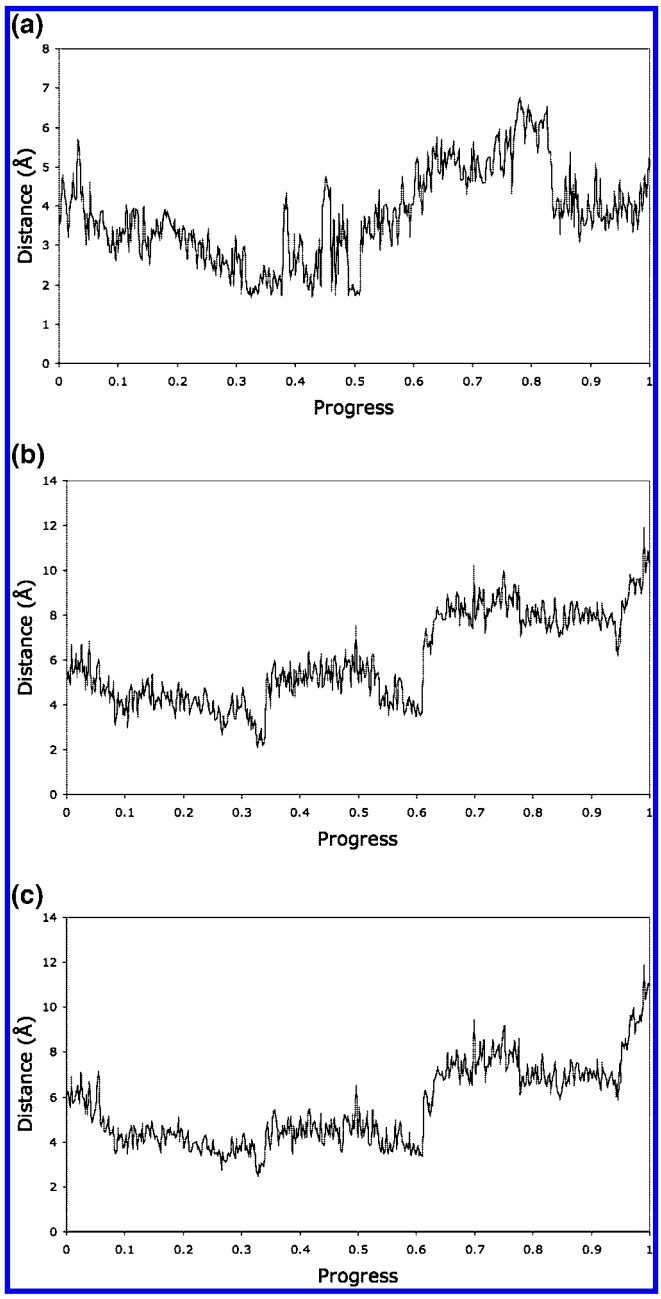

Figure 9. The distance between (a) hydroxyl HG of Ser 275 and hydroxyl O7 of paclitaxel; (b) hydroxyl HG of Ser 278 and carbonyl O10 from the acyl group on C10 of paclitaxel; and (c) hydroxyl HG of Ser 278 and carbonyl C22 from the acyl group on C10 of paclitaxel.

ments indicated that all the paclitaxel molecules were bound to microtubules; in addition Diaz et al.[9] have referred to experiments indicating that there is no difference in rates of paclitaxel binding between tubulin isotypes. The apparent contradiction between these observations and the differing effects of paclitaxel may be explained by the fast binding to the intermediate site allowing paclitaxel to be continuously bound.

A second binding event was observed in the kinetic studies of Diaz et al.,[9] possibly corresponding to the relocation of paclitaxel from the intermediate binding site to the luminal location. This occurred on a time scale on the order of a second, which corresponds to the time scale on which paclitaxel can modify the flexibility of microtubules. The difference between the kinetic pathways in microtubules

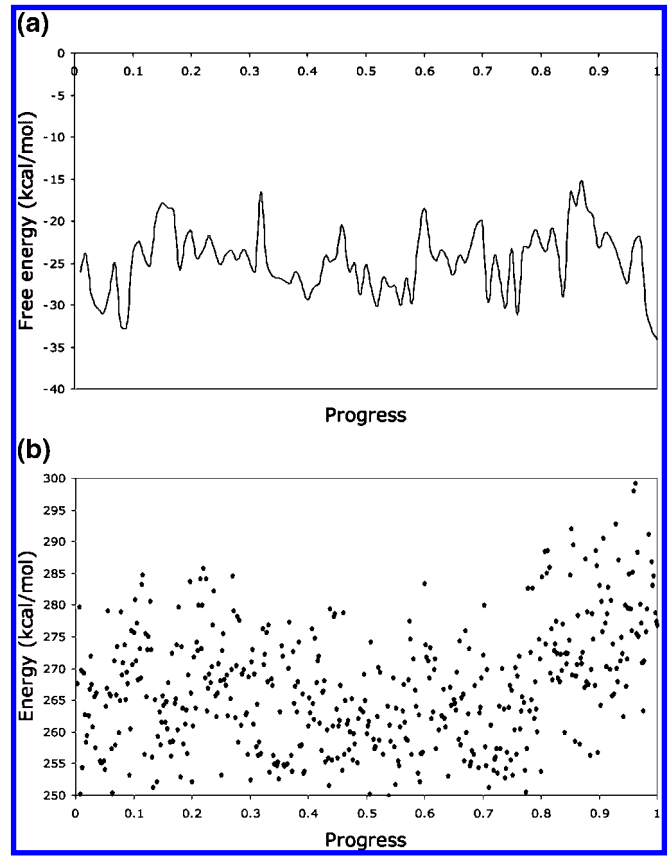

Figure 10. (a) Binding free energies along the TMD trajectory from the intermediate binding site to the observed binding site and (b) internal energies of H6/H7 loop including flanking residues, i.e. the energy of residues 212−223 of β-tubulin, during the motion between binding sites.

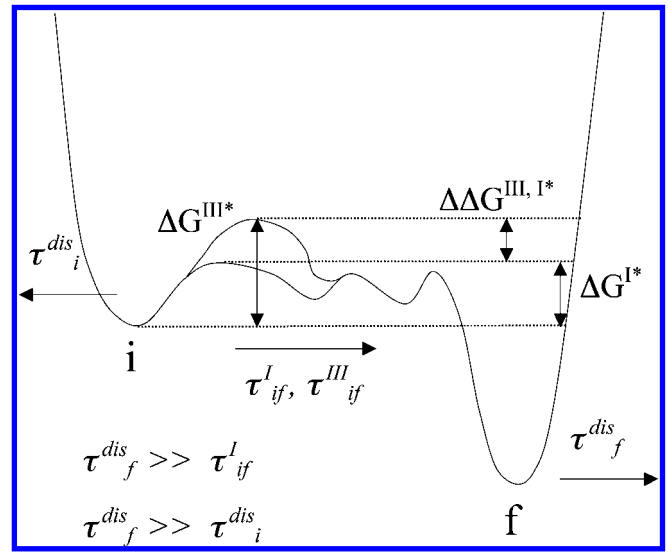

Figure 11. Qualitative potential of mean force profiles for minimum energy paths taken by paclitaxel between intermediate and final binding sites, compared for microtubules composed of βI and βIII tubulin isotypes. Wells marked *i* and *f* represent intermediate and final binding sites characterized by dissociation constants $\tau^{dis}{}_i$ and $\tau^{dis}{}_f$, respectively. The difference $\Delta\Delta G^{III,\ I*}$ between free energy barriers ΔG^{III*} and ΔG^{I*} for the two paths gives rise to different time constants τ^{I}_{if} and τ^{III}_{if}, for the transition of paclitaxel between binding sites in the two isotypes.

composed of βI and βIII tubulin is illustrated schematically in Figure 11. Without the hydrogen bond between paclitaxel and the M-loop, the free energy barrier for the passage of

paclitaxel between the intermediate and final binding sites is increased by the amount $\Delta\Delta G^{III,I^*}$, decreasing the rate constant by a factor of $\exp(\Delta\Delta G^{III,I^*}/kT)$. Since a hydrogen bond typically contributes a free energy of about −5 kcal/mol, in βIII microtubules the time frame for passage between the two binding sites may be expected to increase by 2 to 3 orders of magnitude, to reach a scale of minutes or even hours. This is comparable to the time scale on which microtubule dynamicity occurs, which is significant since tubulin dimers are continually being exchanged in destabilized microtubules. When paclitaxel is located at the intermediate binding site, the alternate paths of microtubule depolymerization, or paclitaxel dissociation from the intermediate binding site (τ^{dis}_i), compete with passage to the final binding site (τ^{I}_{if}, τ^{III}_{if}), where the activity of the drug can take effect. Thus, a significant difference between the values of time constants τ^{I}_{if} and τ^{III}_{if} may result in an insufficient number of drug molecules being able to reach the final binding site where they can halt microtubule depolymerization.

As indicated in Figure 11, once paclitaxel has reached its final binding site, its time constant for dissociation is long compared to the time scales for the competing events occurring at the intermediate binding site, including dissociation, or passage to the final binding site. This makes it difficult to use experimental dissociation kinetic studies or equilibrium data to probe the population of paclitaxel located at the intermediate binding site. Instead, experiments aimed at determining association kinetics in microtubules prepared from purified tubulin isotypes may be performed to validate or contest the predictions of the present study. In addition, comparisons of paclitaxel activity in such microtubules or in microtubules formed from tubulin with single point mutations introduced at residue 275 would be valuable. As mentioned above, the work of Derry et al.[41] compared the sensitivity to paclitaxel between βII microtubules and βIII microtubules. Experiments were performed over a time period of about 10 min or until microtubules underwent complete depolymerization. If the time scale for paclitaxel reaching its final binding site increases to tens of minutes for βIII tubulin, then within 10 min only a fraction of paclitaxel molecules would be expected to become bound at the luminal binding site, in concurrence with the measured factor of 4.6 for the change in activity.

Design of Novel Paclitaxel Derivatives. Knowledge of the structure of the intermediate binding site and the path to the binding site should be considered in relation to the optimization of paclitaxel derivatives. Because our simulations indicate that the movement of paclitaxel between the two binding sites is stabilized by the formation of a hydrogen bond between β-tubulin's serine 275 and paclitaxel's O7, this suggests specific modifications of the drug that may possibly lead to better uptake at the binding site. With an aim at reversing the observed isotype specificity, it may be beneficial to substitute the C7-OH with a nonpolar group or with hydrogen to form the C7-deoxy derivative. In this way the substituted group may better interact with the Ala 275 side chain of βIII tubulin, compared to with the polar side chain of Ser 275 of βI tubulin, potentially reducing the overall activity of paclitaxel in microtubules composed of βI and II tubulin relative to that for microtubules composed of βIII tubulin, found in paclitaxel-resistant cancer cell types.

A few reports exist in the literature as to the relative activity of the C7-deoxy paclitaxel derivative compared to paclitaxel. In tubulin assembly assays, this derivative was found to be slightly less active than paclitaxel,[61] and it has been found to have reduced or similar cytotoxicity in certain cell lines.[61,62] Since βI is the most common β-tubulin isotype, it is likely that this isotype was present in largest abundance in the experiments, in which case these results would confirm the predictions of the present work. However, it is difficult to assess how these observations reflect on the speculations made in the present work without information on specific isotype contents in the cell lines used, and so this is an issue that needs to be investigated further.

From the targeted MD trajectory, it could be noted that the acyl group on C10 of paclitaxel is in a position to possibly be stabilized during the transition by the side chain hydroxyl group of serine 278, if substituted for by a somewhat more extended group. In Figure 9b and Figure 9c, the distances between hydroxyl HG of Ser 278 and carbonyl O10 or C22, respectively, from the acyl group on C10 of paclitaxel, are plotted against trajectory progress. Similar to the interaction between hydroxyl HG of Ser 275 and hydroxyl O7 of paclitaxel, the distances shown display decreased values starting at the point when the motion progress has reached a value of about 0.2, with minimum values of 2.1 Å and 2.5 Å, respectively. Thus, another viable strategy would be to attempt to increase the kinetic rate constant of the transition between sites by replacement of the AcO group on C10 with a group that might form a hydrogen bond with or otherwise be stabilized by the hydroxyl side chain of serine 278.

In a recent work by Matesanz et al.,[63] propionyl groups were substituted for the hydroxyl and acetyl groups on C7 and C10, respectively; in addition, the effect of a hydroxyl substitution at C10 was examined. The change in binding affinity was slight for the C7 modification and even smaller for the modifications at C10. This is not surprising as the C10 acetyl group faces outward from the binding interface, without interaction with tubulin, in the luminal-binding site. On the other hand, the propionyl substitution at C7 increased the IC50 by more than an order of magnitude, as did the hydroxyl (but not the propionyl) at C10. One possible explanation for these findings is that the propionyl or hydroxyl substitutions at C7 and C10, respectively, destabilize the path taken by the taxane between the intermediate and final binding sites and would seem to indicate that a C10 acetyl or propionyl group may be stabilized during this path by hydrophobic interaction with tubulin. This is consistent with the results of our computer simulations presented in this paper.

CONCLUSION

This paper has been concerned with how the microtubule structure may affect the ability of paclitaxel to bind at its binding site in the lumen. The results of our modeling show that it is likely that the drug passes through an intermediate binding site and that specific residues may be critical to allowing paclitaxel to move from here to its binding site. In particular, our docking calculation positioned the paclitaxel binding site within the pore in the same region previously predicted by Diaz et al.,[9] in a conformation amenable to flipping over the H6−H7 loop into the binding site as had

been proposed. Moreover, Brownian dynamics simulations to the intermediate binding site produced a value close to that of the observed rate constant. Finally, a targeted molecular dynamics simulation, with an external force to facilitate motion between the two binding sites, suggests that this pathway is stabilized by a hydrogen bond between Ser 275 on the M-loop of β tubulin and paclitaxel's C7 OH. We have made suggestions for the derivatization of the paclitaxel molecule that could overcome the well-known drug resistance effects in a large subpopulation of cancer patients and lead to improved therapeutic outcomes.

Abbreviations: GDP, guanosine diphosphate; GTP, guanosine triphosphate; MD, molecular dynamics; MM-GBSA, molecular-mechanics Generalized-Born-surface-area; rmsd, root-mean-square deviation; SDA, simulation of diffusional association; TMD, targeted molecular dynamics.

ACKNOWLEDGMENT

We thank Eric Carpenter for providing tubulin isotype structures, Dr. Razif Gabdoulline and Dr. Rebecca Wade for assistance with the SDA program, and Prof. Peter Tieleman for discussion. This work was supported by grants to J.A.T. from the Allard Foundation, the Alberta Cancer Board, and NSERC; by Pacific Institute of Mathematical Sciences and Bhatia Foundation fellowships to H.F.; and by grants to R.F.L. from the United States Army Breast Cancer Research Program (W81XWH-05-1-0238), the San Antonio Cancer Institute (P30 CA54174), the State of Texas Higher Coordinating Board, and the Welch Foundation (AQ-0726).

Supporting Information Available: Lists of residues making up the four different kinds of microtubule pores, constructed for the αIV/βI microtubule (Table S1); contributions of individual residues within the final binding site (excluding the M-loop) to total binding free energy, in kcal/mol (Table S2); and dipole used in Brownian dynamics with charges given in atomic units and radii given in angstroms (Figure S1). This material is available free of charge via the Internet at http://pubs.acs.org.

REFERENCES AND NOTES

(1) Mitchison, T.; Kirschner, M. Dynamic instability of microtubule growth. *Nature* **1984**, *312*, 237–242.
(2) Jordan, M.; Wendell, K.; Gardiner, S.; Derry, W.; Copp, H.; Wilson, L. Mitotic block induced in HeLa cells by low concentrations of paclitaxel (Taxol) results in abnormal mitotic exit and apoptotic cell death. *Cancer Res.* **1996**, *56*, 816–825.
(3) Wang, H.; Nogales, E. Nucleotide-dependent bending flexibility of tubulin regulates microtubule assembly. *Nature* **2005**, *435*, 911–915.
(4) Xiao, H.; Verdier-Pinard, P.; Fernandez-Fuentes, N.; Burd, B.; Angeletti, R.; Fiser, A.; Horwitz, S.; Orr, G. A. Insights into the mechanism of microtubule stabilization by Taxol. *Proc. Natl. Acad. Sci. U.S.A.* **2006**, *103*, 10166–10173.
(5) Li, H.; Derosier, D.; Nicholson, W.; Nogales, E.; Downing, K. Microtubule structure at 8 A resolution. *Structure (Cambridge)* **2002**, *10*, 1317–1328.
(6) Odde, D. Diffusion inside microtubules. *Eur. Biophys. J.* **1998**, *27*, 514–520.
(7) Ross, J.; Fygenson, D. Mobility of taxol in microtubule bundles. *Biophys. J.* **2003**, *84*, 3959–3967.
(8) Buey, R.; Calvo, E.; Barasoain, I.; Pineda, O.; Edler, M.; Matesanz, R.; Cerezo, G.; Vanderwal, C.; Day, B. W.; Sorensen, E.; Lopez, J.; Andreu, J.; Hamel, E.; Diaz, J. Cyclostreptin binds covalently to microtubule pores and lumenal taxoid binding sites. *Nat. Chem. Biol.* **2007**, *3*, 117–125.
(9) Diaz, J.; Barasoain, I.; Andreu, J. Fast kinetics of Taxol binding to microtubules. Effects of solution variables and microtubule-associated proteins. *J. Biol. Chem.* **2003**, *278*, 8407–8419.
(10) Andreu, J.; Barasoain, I. The interaction of baccatin III with the taxol binding site of microtubules determined by a homogeneous assay with fluorescent taxoid. *Biochemistry* **2001**, *40*, 11975–11984.
(11) Luduena, R. Are tubulin isotypes functionally significant. *Mol. Biol. Cell* **1993**, *4*, 445–457.
(12) Nettles, J.; Li, H.; Cornett, B.; Krahn, J.; Snyder, J.; Downing, K. The binding mode of epothilone A on alpha,beta-tubulin by electron crystallography. *Science* **2004**, *305*, 866–869.
(13) Fiser, A.; Do, R. K.; Sali, A. Modeling of loops in protein structures. *Protein Sci.* **2000**, *9*, 1753–1773.
(14) Ravelli, R.; Gigant, B.; Curmi, P.; Jourdain, I.; Lachkar, S.; Sobel, A.; Knossow, M. Insight into tubulin regulation from a complex with colchicine and a stathmin-like domain. *Nature* **2004**, *428*, 198–202.
(15) Lowe, J.; Li, H.; Downing, K.; Nogales, E. Refined structure of alpha beta-tubulin at 3.5 A resolution. *J. Mol. Biol.* **2001**, *313*, 1045 1057.
(16) Carpenter, E.; Huzil, J.; Luduena, R.; Tuszynski, J. Homology modeling of tubulin: influence predictions for microtubule's biophysical properties. *Eur. Biophys. J.* **2006**, *36*, 35–43.
(17) Huzil, J.; Luduena, R.; Tuszynski, J. Comparative modelling of human beta-tubulin isotypes and implications for drug binding. *Nanotechnology* **2006**, *17*, S90−S100.
(18) Humphrey, W.; Dalke, A.; Schulten, K. VMD: visual molecular dynamics. *J. Mol. Graphics* **1996**, *14*, 33–38.
(19) Frisch, M. J.; Trucks, G. W.; Schlegel, H. B.; Scuseria, G. E.; Robb, M. A.; Cheeseman, J. R.; Montgomery, J. A., Jr.; Vreven, T.; Kudin, K. N.; Burant, J. C.; Millam, J. M.; Iyengar, S. S.; Tomasi, J.; Barone, V.; Mennucci, B.; Cossi, M.; Scalmani, G.; Rega, N.; Petersson, G. A.; Nakatsuji, H.; Hada, M.; Ehara, M.; Toyota, K.; Fukuda, R.; Hasegawa, J.; Ishida, M.; Nakajima, T.; Honda, Y.; Kitao, O.; Nakai, H.; Klene, M.; Li, X.; Knox, J. E.; Hratchian, H. P.; Cross, J. B.; Bakken, V.; Adamo, C.; Jaramillo, J.; Gomperts, R.; Stratmann, R. E.; Yazyev, O.; Austin, A. J.; Cammi, R.; Pomelli, C.; Ochterski, J. W.; Ayala, P. Y.; Morokuma, K.; Voth, G. A.; Salvador, P.; Dannenberg, J. J.; Zakrzewski, V. G.; Dapprich, S.; Daniels, A. D.; Strain, M. C.; Farkas, O.; Malick, D. K.; Rabuck, A. D.; Raghavachari, K.; Foresman, J. B.; Ortiz, J. V.; Cui, Q.; Baboul, A. G.; Clifford, S.; Cioslowski, J.; Stefanov, B. B.; Liu, G.; Liashenko, A.; Piskorz, P.; Komaromi, I.; Martin, R. L.; Fox, D. J.; Keith, T.; AlLaham, M. A.; Peng, C. Y.; Nanayakkara, A.; Challacombe, M.; Gill, P. M. W.; Johnson, B.; Chen, W.; Wong, M. W.; Gonzalez, C.; Pople, J. A. *Gaussian 03*; Gaussian, Inc.: Wallingford, CT, 2004.
(20) Morris, G. M.; Goodsell, D. S.; Halliday, R. S.; Huey, R.; Hart, W. E.; Belew, R. K.; Olson, A. J. Automated Docking Using a Lamarckian Genetic Algorithm and and Empirical Binding Free Energy Function. *J. Comput. Chem.* **1998**, *16*, 1639–1662.
(21) Baker, N.; Sept, D.; Joseph, S.; Holst, M.; Mccammon, J. Electrostatics of nanosystems: application to microtubules and the ribosome. *Proc. Natl. Acad. Sci. U.S.A.* **2001**, *98*, 10037–10041.
(22) Gabdoulline, R.; Wade, R. Simulation of the diffusional association of barnase and barstar. *Biophys. J.* **1997**, *72*, 1917–1929.
(23) Gabdoulline, R.; Wade, R. Brownian dynamics simulation of protein-protein diffusional encounter. *Methods* **1998**, *14*, 329–341.
(24) Diaz, J.; Strobe, R.; Engelborghs, Y.; Souto, A.; Andreu, J. Molecular recognition of taxol by microtubules. Kinetics and thermodynamics of binding of fluorescent taxol derivatives to an exposed site. *J. Biol. Chem.* **2000**, *275*, 26265–26276.
(25) Sigalov, G.; Fenley, A.; Onufriev, A. Analytical electrostatics for biomolecules: beyond the generalized Born approximation. *J. Chem. Phys.* **2006**, *124*, 124902.
(26) Bereolos, P.; Talbot, J.; Allen, M. P.; Evans, G. T. Transport properties of the hard ellipsoid fluid. *J. Chem. Phys.* **1993**, *99*, 6087–6097.
(27) Hu, C.-M.; Zwanzig, R. Rotational friction coefficients for spheroids with the slipping boundary condition. *J. Chem. Phys.* **1974**, *60*, 4354–4357.
(28) Case, D.; Cheatham, T. R.; Darden, T.; Gohlke, H.; Luo, R.; Merz, K. J.; Onufriev, A.; Simmerling, C.; Wang, B.; Woods, R. The Amber biomolecular simulation programs. *J. Comput. Chem.* **2005**, *26*, 1668–1688.
(29) Duan, Y.; Wu, C.; Chowdhury, S.; Lee, M. C.; Xiong, G.; Zhang, W.; Yang, R.; Cieplak, P.; Luo, R.; Lee, T.; Caldwell, J.; Wang, J.; Kollman, P. A point-charge force field for molecular mechanics simulations of proteins based on condensed-phase quantum mechanical calculations. *J. Comput. Chem.* **2003**, *24*, 1999–2012.
(30) Cornell, W. D.; Cieplak, P.; Bayly, C. I.; Gould, I. R.; Merz, K. M.; Ferguson, D. M.; Spellmeyer, D. C.; Fox, T.; Caldwell, J. W.; Kollman, P. A. A second generation force field for the simulation of proteins, nucleic acids, and organic molecules. *J. Am. Chem. Soc.* **1995**, *117*, 5179–5197.
(31) Meagher, K.; Redman, L.; Carlson, H. Development of polyphosphate parameters for use with the AMBER force field. *J. Comput. Chem.* **2003**, *24*, 1016–1025.

(32) Jorgensen, W. L.; Chandrasekhar, J.; Madura, J. D.; Impey, R. W.; Klein, M. L. Comparison of simple potential functions for simulating liquid water. *J. Chem. Phys.* **1983**, *79*, 926–935.

(33) Berendsen, H. J. C.; Postma, J. P. M.; Gunsteren, W. F. v.; Dinola, A.; Haak, J. R. Molecular dynamics with coupling to an external bath. *J. Chem. Phys.* **1984**, *81*, 3684–3690.

(34) Ryckaert, J. P.; Ciccotti, G.; Berendsen, H. J. C. Numerical integration of Cartesian equations of motion of a system with constraints: molecular dynamics of n-alkanes. *J. Comput. Phys.* **1977**, *23*, 327–341.

(35) Huzil, J. T.; Chen, K.; Kurgan, L.; Tuszynski, J. A. The Roles of β-Tubulin Mutations and Isotype Expression in Acquired Drug Resistance. *Cancer Inf.* **2007**, *3*, 159–181.

(36) Westermann, S.; Wang, H.; AvilaSakar, A.; Drubin, D.; Nogales, E.; Barnes, G. The Dam1 kinetochore ring complex moves processively on depolymerizing microtubule ends. *Nature* **2006**, *440*, 565–569.

(37) Barlow, S.; Gonzalez-Garay, M. L.; Cabral, F. Paclitaxel-dependent mutants have severely reduced microtubule assembly and reduced tubulin synthesis. *J. Cell Sci.* **2002**, *115*, 3469–3478.

(38) Giannakakou, P.; Gussio, R.; Nogales, E.; Downing, K.; Zaharevitz, D.; Bollbuck, B.; Poy, G.; Sackett, D.; Nicolaou, K.; Fojo, T. A common pharmacophore for epothilone and taxanes: molecular basis for drug resistance conferred by tubulin mutations in human cancer cells. *Proc. Natl. Acad. Sci. U.S.A.* **2000**, *97*, 2904–2909.

(39) Gonzalez-Garay, M. L.; Chang, L.; Blade, K.; Menick, D.; Cabral, F. A beta-tubulin leucine cluster involved in microtubule assembly and paclitaxel resistance. *J. Biol. Chem.* **1999**, *274*, 23875–23882.

(40) Monzo, M.; Rosell, R.; Sanchez, J.; Lee, J. S.; O'brate, A.; Gonzalez-Larriba, J. L.; Alberola, V.; Lorenzo, J.; Nunez, L.; Ro, J. Y.; Martin, C. Paclitaxel resistance in non-small-cell lung cancer associated with beta-tubulin gene mutations. *J. Clin. Oncol.* **1999**, *17*, 1786–1793.

(41) Derry, W.; Wilson, L.; Khan, I.; Luduena, R.; Jordan, M. Taxol differentially modulates the dynamics of microtubules assembled from unfractionated and purified beta-tubulin isotypes. *Biochemistry* **1997**, *36*, 3554–3562.

(42) Schlitter, J.; Engels, M.; Kruger, P. Targeted molecular dynamics: a new approach for searching pathways of conformational transitions. *J. Mol. Graphics* **1994**, *12*, 84–89.

(43) Isralewitz, B.; Gao, M.; Schulten, K. Steered molecular dynamics and mechanical functions of proteins. *Curr. Opin. Struct. Biol.* **2001**, *11*, 224–230.

(44) Scott, C.; Walker, C.; Neal, D.; Harper, C.; Bloodgood, R.; Somers, K.; Mills, S.; Rebhun, L.; Levine, P. Beta-tubulin epitope expression in normal and malignant epithelial cells. *Arch. Otolaryngol. Head Neck Surg.* **1990**, *116*, 583–589.

(45) Ranganathan, S.; Dexter, D.; Benetatos, C.; Chapman, A.; Tew, K. D.; Hudes, G. Increase of beta(III)- and beta(IVa)-tubulin isotopes in human prostate carcinoma cells as a result of estramustine resistance. *Cancer Res.* **1996**, *56*, 2584–2589.

(46) Kavallaris, M.; Kuo, D. Y.; Burkhart, C.; Regl, D.; Norris, M.; Haber, M.; Horwitz, S. Taxol-resistant epithelial ovarian tumors are associated with altered expression of specific beta-tubulin isotypes. *J. Clin. Invest.* **1997**, *100*, 1282–1293.

(47) Prasannan, L.; Misek, D.; Hinderer, R.; Michon, J.; Geiger, J.; Hanash, S. Identification of beta-tubulin isoforms as tumor antigens in neuroblastoma. *Clin. Cancer Res.* **2000**, *6*, 3949–3956.

(48) Dozier, J. H.; Hiser, L.; Davis, J.; Thomas, N.; Tucci, M.; Benghuzzi, H.; Frankfurter, A.; Correia, J.; Lobert, S. Beta class II tubulin predominates in normal and tumor breast tissues. *Breast Cancer Res.* **2003**, *5*, R157−R169.

(49) Ferguson, R.; Taylor, C.; Stanley, A.; Butler, E.; Joyce, A.; Harnden, P.; Patel, P.; Selby, P.; Banks, R. Resistance to the tubulin-binding agents in renal cell carcinoma: no mutations in the class I beta-tubulin gene but changes in tubulin isotype protein expression. *Clin. Cancer Res.* **2005**, *11*, 3439–3445.

(50) Mozzetti, S.; Ferlini, C.; Concolino, P.; Filippetti, F.; Raspaglio, G.; Prislei, S.; Gallo, D.; Martinelli, E.; Ranelletti, F.; Ferrandina, G.; Scambia, G. Class III beta-tubulin overexpression is a prominent mechanism of paclitaxel resistance in ovarian cancer patients. *Clin. Cancer Res.* **2005**, *11*, 298–305.

(51) Goncalves, A.; Braguer, D.; Kamath, K.; Martello, L.; Briand, C.; Horwitz, S.; Wilson, L.; Jordan, M. Resistance to Taxol in lung cancer cells associated with increased microtubule dynamics. *Proc. Natl. Acad. Sci. U.S.A.* **2001**, *98*, 11737–11742.

(52) Kamath, K.; Wilson, L.; Cabral, F.; Jordan, M. BetaIII-tubulin induces paclitaxel resistance in association with reduced effects on microtubule dynamic instability. *J. Biol. Chem.* **2005**, *280*, 12902–12907.

(53) Hari, M.; Yang, H.; Zeng, C.; Canizales, M.; Cabral, F. Expression of class III beta-tubulin reduces microtubule assembly and confers resistance to paclitaxel. *Cell Motil. Cytoskeleton* **2003**, *56*, 45–56.

(54) Verdier-Pinard, P.; Wang, F.; Burd, B.; Angeletti, R.; Horwitz, S.; Orr, G. A. Direct analysis of tubulin expression in cancer cell lines by electrospray ionization mass spectrometry. *Biochemistry* **2003**, *42*, 12019–12027.

(55) Burkhart, C.; Kavallaris, M.; Band Horwitz, S. The role of beta-tubulin isotypes in resistance to antimitotic drugs. *Biochim. Biophys. Acta* **2001**, *1471*, O1−O9.

(56) Lu, Q.; Luduena, R. Removal of beta III isotype enhances taxol induced microtubule assembly. *Cell Struct. Funct.* **1993**, *18*, 173–182.

(57) Lobert, S.; Frankfurter, A.; Correia, J. Binding of vinblastine to phosphocellulose-purified and alpha beta-class III tubulin: the role of nucleotides and beta-tubulin isotypes. *Biochemistry* **1995**, *34*, 8050–8060.

(58) Magnani, M.; Ortuso, F.; Soro, S.; Alcaro, S.; Tramontano, A.; Botta, M. The betaI/betaIII-tubulin isoforms and their complexes with antimitotic agents. Docking and molecular dynamics studies. *FEBS J.* **2006**, *273*, 3301–3310.

(59) Rezania, V.; Azarenko, O.; Jordan, M.; Bolterauer, H.; Luduena, R.; Huzil, J.; Tuszynski, J. Microtubule assembly of isotypically purified tubulin and its mixtures. *Biophys. J.* **2008**, *95*, 1993–2008.

(60) Newton, C.; Deluca, J. G.; Himes, R. H.; Miller, H. P.; Jordan, M.; Wilson, L. Intrinsically slow dynamic instability of HeLa cell microtubules in vitro. *J. Biol. Chem.* **2002**, *277*, 42456–42462.

(61) Ge, H.; Vasandani, V.; Huff, J. K.; Audus, K. L.; Himes, R. H.; Seelig, A.; Georg, G. I. Synthesis and interactions of 7-deoxy-, 10-deacetoxy, and 10-deacetoxy-7-deoxypaclitaxel with NCI/ADR-RES cancer cells and bovine brain microvessel endothelial cells. *Bioorg. Med. Chem. Lett.* **2006**, *16*, 433–436.

(62) Chen, S.-H.; Kant, J.; Mamber, S. W.; Roth, G. P.; Wei, J.-M.; Marshall, D.; Vyas, D. M.; Farina, V.; Casazza, A.; Long, B. H.; Rose, W. C.; Johnston, K.; Fairchild, C. Taxol structure-activity relationships: synthesis and biological evaluation of taxol analogs modified at C-7. *Bioorg. Med. Chem. Lett.* **1994**, *4*, 2223–2228.

(63) Matesanz, R.; Barasoain, I.; Yang, C.-G.; Wang, L.; Li, X.; De Concepciûn, I.; Coderch, C.; Gago, F.; Barbero, J. J.; Andreu, J. M.; Fang, W.-S.; Dìaz, J. F. Optimization of Taxane Binding to Microtubules: Binding Affinity Dissection and Incremental Construction of a High-Affinity Analog of Paclitaxel. *Chem. Biol.* **2008**, *15*, 573–585.

(64) Delano, W. L. *The PyMOL Molecular Graphics System*; DeLano Scientific: San Carlos, CA, 2002.

CI8003336